

INTEGRATED TURNING-RAY AND REFLECTION TOMOGRAPHY
FOR VELOCITY MODEL BUILDING IN FOOTHILL AREAS

Tian Jun and Peng Gengxin,

{Tarim Oilfield Company, PetroChina, Korla, China,

tianjun-tlm@petrochina.com.cn , penggx-tlm@petrochina.com.cn }

Junru Jiao, Grace (Yan) Yan and Xianhuai Zhu,

{Forland Geophysical Services (FGS), Houston, USA

jjiao@forlandgeo.com, yyan@forlandgeo.com, xzhu@forlandgeo.com, }

Original paper date of submission: 12/31/2017

Revised paper date of submission: 05/31/2018

ABSTRACT

A special challenge for land seismic exploration is estimating velocities, in part due to complex near surface structures, and in some instances because of rugose topography over foothills. We propose an integrated turning-ray and reflection tomographic method to face with the challenge. First, turning-ray tomography is performed to derive a near-surface velocity-depth model. Then, we combine the near-surface model with the initial-subsurface model. Taking the combined model as starting model, we go through a reflection tomographic process to build the model for imaging. During reflection tomography, both near surface model and subsurface models are jointly updated. The proposed method has been successfully applied to a 2D complex synthetic data example and a 3D field data example. The results demonstrate that the proposed method derives a very decent model even when there is no reflection information available in a few hundred meters underneath surface. Joint tomography can lead to geological plausible models and produce subsurface images with high fidelity.

INTRODUCTION

Reflection tomography in the post-migration domain has dominated the advantages of velocity model building in seismic imaging, especially for marine seismic exploration where the near surface model is not problematic. Reflection tomography is challenged to derive a near surface model with high quality because there are only very limited valid traces, or no valid traces, in near surface up to a few hundred meters in depth from the surface. An alternative method is desirable to obtain a reliable near-surface velocity-depth model. Here, we propose the

integrated method of turning-ray tomography and reflection tomography to build velocity model for foothill exploration. First, we pick first breaks as input for turning-ray tomography to derive the near-surface velocity-depth model. An initial subsurface depth model is obtained by converting RMS velocities into interval velocities in depth domain. Then, we merge the near-surface velocity-depth model with the initial model as the starting velocity model for anisotropic reflection tomography. We tested the proposed method on a complex 2D synthetic data example, and then applied it to a 3D field data set from foothills of western China.

PRINCIPLE OF INTEGRATED TOMOGRAPHY

Zhu et al. (2001, 2003) and Song et al., (2014), among others, proposed a joint tomography combining both refraction or turning-ray tomography and reflection tomography to build an entire velocity model for depth migration. Turning-ray tomography has been conventionally used to calculate statics, which is also referred to as tomostatics (Zhu, et al., 1992; Bell et al., 1994; Stefani, 1995; Zhang et al., 2006). In turning-ray tomography, the medium to be imaged is generalized into a continuous medium, such that the first arrivals recorded at the surface need not be associated with refractors having strong velocity contrasts. Turning-ray tomography inverts for a velocity model by minimizing misfits between observed first-break times and calculated travel times from turning-rays. Since a continuous medium is assumed, the inversion results in a grid-based model. Usually, turning ray tomography can robustly invert models with depth up to one-fourth of recording aperture (signed offsets). Very often turning ray penetrates deeper than refraction ray because refraction requires velocities to increase with depth while turning wave does not need this requirement, provided that the earth

has an overall positive velocity gradient due to compaction of rocks and the recording aperture is sufficient enough to allow rays turning back to the surface. We can use this model as a good estimation of near surface model combined with reflection tomography. However, in practice, we need to select maximum depths of reliable velocities according to ray density for every location.

Reflection tomography in the post-migration domain utilizes depth residuals among traces within a common image gather generated from prestack depth migration (Stork, C., 1992; Jiao, et al., 2009, 2010; Sherwood, et al., 2011). The residuals are distributed along reflection rays. By minimizing the residuals, reflection tomography inverts for perturbation of velocity and other anisotropic parameters and then updates models according to the previous models. Reflection tomography is an iterative process of prestack depth migration and tomographic inversion until the residuals are diminished since linearization is applied.

Since the near-surface velocity-depth model derived from turning-ray tomography is more accurate and has higher resolution than that from reflection tomography beneath the surface, we keep this model unchanged during early stages of iterations in the integrated tomography. To account for the errors associated with the picked first arrivals for turning-ray tomography and combine both models seamlessly, we allow reflection tomography to update both shallow and deep velocities simultaneously in the later stage of iterations. Reflection tomography is a global inversion. At early stages of model building, errors in estimation of models are larger in deeper areas than in shallower areas. The errors in deeper areas affect shallower areas. To avoid error transfer to the near surface model derived by the turning ray tomography, the near surface model

is masked in the first several iterations. After a few iterations of reflection tomography, the errors are reduced. Then, reflection tomography updates velocity and anisotropic parameters in both shallower and deeper areas.

SYNTHETIC DATA EXAMPLE

We first applied the proposed method and workflow to a 2D synthetic dataset which simulates Canadian Foothills (Boonyasiriwat, et al. 2009). The model has a dimension of 20 km in the crossline direction and 6.5 km in depth. It has rugose topography with elevation relief up to 700 meters, and subsurface geological structures are also complicated. The very specific feature of the model is that there are no reflection layers within 600 meters underneath the surface, which makes it very difficult to derive near surface model by reflection tomography. We first picked the first arrivals from common shot gathers, then performed turning-ray tomography. Figures 1 and 2 show the ray density and inverted near-surface velocity-depth model, respectively. According to the distribution of ray density in Figure 1, we picked a horizon as the maximum depth for reliable velocities. The maximum thickness of inverted model is approximately 1200 meters from the topography. To create an initial model for prestack depth migration, we heavily smoothed the true velocity model in both horizontal and vertical directions, scaled velocities by 0.95 and then combined it with the near-surface model. At the suture zone (defined by the dotted line based on the ray-density QC plot as showed in Figure 1), tapering was applied to avoid abrupt changes. This combined model is presented in Figure 3.

Beginning with the initial combined model, we perform migration and reflection tomography iterations. We use Kirchhoff prestack depth migration to generate common image

gathers in the offset-depth domain. The offsets of gathers are from 100 meters to 7900 meters with an increment of 200 meters and the depth is to 6500 meters with an interval of 5 meters. Figure 4 shows the common image gathers (CIG) at selected crosslines after prestack depth migration using the initial velocity model. Most events are curved up and also show non-hyperbolic residual moveout, since the true velocities are scaled by 0.95 and the model has strongly vertical and lateral velocity variations. The stacked migration from the initial model is showed in Figure 5.

In this example during the first three tomographic iterations, we keep the near surface part unchanged by applying masking function in the inversion. Later, we allow reflection tomography to update both near-surface and subsurface areas simultaneously. We find that reflection tomography adds more details into the near surface model. After several iterations, flatness of CIG has been improved significantly, and more details are revealed for the velocity model. Figures 6 and 7 show the selected common image gathers and stack from the final inverted model in Figure 8. For comparison, we also present the true velocity model and the corresponding stacked migration section in Figure 9, and Figure 10, respectively. Although the inverted model is quite smooth, it shows the major features of true model. Comparing stacked migrations from the initial model, the inverted model, and the true model, the image from the inverted model removes the “fake structures” marked by the white and yellow rectangles and caused by inaccurate initial model. The overthrust feature in the middle of the model (circle in Figure 8) after integrated tomography is also evident.

FIELD EXAMPLE

We have applied the proposed methods to several field projects. Here, we take Keshen project as an example. The area is located at Tarim Basin, northwestern of China where a set of thrust faults were pushed southward by the northern Tianshan orogeny, which resulted in rugged topography with steep slopes, dipping outcrops (maximum more than 80 degrees), and the relative elevation variation from 500 to 1000 m. Figure 11 shows a Schematic geological vertical section for the studying area. Figure 12 is the elevation map of studying area. The near-surface morphology of the study area is known to have isolated high-velocity conglomerate rocks in the foreland basin surrounded by weathered sediments. The targeted zones are at depth of ~ 7 km underneath the conglomerate rocks. .

To estimate more accurate models and obtain image with high fidelity, we first derive the near-surface velocity-depth model and combine it with the legacy depth model. Then using the combined model as the starting model, we perform iterative reflection TTI tomography and prestack depth migration for anisotropic model building. The resultant near surface model is shown in Figure 13a for one inline and Figure 13b for depth slice at depth of 900 meters . The marked high-velocity zone corresponds to conglomerate rocks and is consistent and compatible with the geological background of the study area. A “reliable depth” from turning-ray tomographic solution can reach approximately down to 1500m from topography (dashed line in Figure 13a) which is much deeper than one from conventional refraction inversion. Figure 14 shows the combined model. From the final datum to the surface, a constant replacement velocity is used. From surface to the reliable depth (the red dash line in Figure 14), we use the velocity

from turning ray tomography. The deeper area is filled with the legacy model previously obtained. There is a transient zone between the near-surface and legacy models.

During first three iterations, we keep the near-surface model unchanged while we update both models in the last two iterations. Figure 15 compares the final velocity model with the starting one located at one inline. Figure 16 compares the initial epsilon and inverted epsilon overlaid with the stacked PSDM respectively located at the same inline as in Figure 16. The updated models reveal more details. After TTI tomography, near surface velocities are reduced while anisotropic parameter epsilon is increased. Although the initial epsilon is constant, the inverted epsilons vary both vertically and laterally consistent with imaged structures. The inverted epsilons are larger in dipping layers than that in horizontal layers. At shallow areas, inverted epsilons are larger than the initial ones. This case demonstrates that isotropic turning ray tomography leads to higher estimation of velocity due to the existence of anisotropy. The migrated results from the updated models are shown in Figure 17. This representative inline is overlaid with Well KS12. The new apex of the structure (blue line cutting through) is now on the right side of the previously drilled location (yellow dashed line), several hundred meters apart. The well drilled previously missed the target, only water was discovered in the reservoir. A new well location was suggested according to the current processing.

After the application of TTI reflection tomography (Zhou, et al., 2011), the velocities near the surface have been slightly reduced. This is because in isotropic turning-ray tomography, which was used in this study, the near-surface velocities will be overestimated if the media near the surface are anisotropic. Turning rays contain substantial horizontal component. TTI reflection tomography can compensate for the horizontal component. Figure 18 and Figure 19

compare the common image gathers from the initial models and the updated models. The flatness of events improves significantly overall, which demonstrates that anisotropic tomography is necessary to derive multiple anisotropic parameters for imaging.

CONCLUSIONS

We have proposed a method of integrated turning-ray and reflection tomography to build models, using a different constraint strategy. The proposed method faces with difficulty of estimating near-surface model in land seismic imaging. We first use turning-ray tomography to derive the near-surface velocity-depth model using the first arrivals as input. Then, reflection tomography is performed to invert for the subsurface model with near surface model masked at first several iterations. During later iterations, both near and subsurface models are updated. We found that near-surface velocities are decreased after integrated inversion. The percentage of velocity reduction depends upon the degree of anisotropy near the surface. We have applied the proposed method to both complex 2D synthetic data set and 3D field data set successfully. Both examples show that turning-ray tomography produces more accurate and higher resolution near-surface velocity-depth models with deeper penetration than that from conventional refraction inversion, and the integrated turning-ray and reflection tomographic inversion lead to the geological plausible models thence produce subsurface image with higher fidelity.

ACKNOWLEDGEMENTS

We thank Allen Bertagne, Sherman Yang, Lei Fu, Bin Yang and John Gillooly for valuable discussions. We also thank Tarim Oilfield Company of PetroChina and Forland Geophysical

Services for permission to publish this work. Constructive suggestions and comments from the anonymous reviewers are very much appreciated.

REFERENCES

Bell, M. L., Lara R., and Gray W. C., (1994), Application of turning-ray tomography to the offshore Mississippi delta: SEG Technical Program Expanded Abstracts, 1509-1512.

Boonyasiriwat, C., Valasek, P., Routh, P., and Zhu, X, 2009, Application of multiscale waveform tomography for high-resolution velocity estimation in complex geologic environments: Canadian Foothills synthetic data example: The Leading Edge, April 2009, 454-456.

Jiao, J., Lin, S., Zhou, C., Brandsberg-Dahl, S., Schleicher, K., and Tieman, H. (2009), Multi-parameter controlled automatically picking and variable smoothing for tomography with fast 3D beam prestack depth migration, 79th SEG Annual Meeting.

Jiao, J., Zhou, C., D., Lin, S., Van der Burg, D., and Brandsberg-Dahl, S. (2010), Velocity model building strategy for multi-azimuth surveys, 80th SEG Annual Meeting.

Sherwood, J., Jiao*, J., Tieman, H., Sherwood, K., Zhou, C., Lin, S., and Brandsberg-Dahl, S. (2011), Hybrid tomography based on beam migration, 81st SEG Annual Meeting.

Stefani, J. P., 1995, Turning-ray tomography: Geophysics, 60, 1917-1929.

Song, M., Liu, X., Han, X., Wang, D., Yang, S., and Hinz, C., 2014, Combining diving-wave tomography and prestack reflection tomography for complex depth imaging – A case study from mountainous western China: *The Leading Edge*, 33 (8), 868-874.

Stork, C., 1992, Reflection tomography in the post migrated domain: *Geophysics, Soc. of Expl. Geophys.*, 57, 680-692.

Zhang, J., O. Yilmaz, and N. Dai, 2006, First-arrival tomostatics and residual statics for near-surface corrections, *CSPG-CSEG-CWLS Convention*, 317-321.

Zhou, C., Jiao, J., Lin, S., Sherwood, J., and Brandsberg-Dahl, S. (2011), Multiparameter joint tomography for TTI model building, *Geophysics* 76, 183-190

Zhu, X., A. Huffman and J. Castagna, 2003, Tomography for enhanced geopressure prediction and depth imaging: *SPG/SEG Conference in Beijing*.

Zhu, X., K. D. Wyatt, and A. Lau, 2001, Turning-ray tomography and tomostatics: “Recent Advances and the Road Ahead” session at *SEG Annual Meeting*.

Zhu, X., Sixta, D.P., and Angstman, B.G., 1992, Tomostatics: Turning-ray tomography + static corrections: *The Leading Edge*, 12, 15-23.

LIST OF FIGURES

Include a complete list of figure captions.

Figure 1. Ray density from turning-ray tomography. The dotted line in the deeper part is the horizon for maximum depth of reliable velocities.

Figure 2. Inverted near surface model from turning-ray tomography.

Figure 3. The combined initial model for reflection tomography. Shallow part is from the inverted near-surface model from turning-ray tomography; deep part is from the true velocity model with heavily smoothing and scaling.

Figure 4. The selected common image gathers using the integrated initial velocity model. The arrows show the non-hyperbolic residual moveout. The gathers are in the depth-offset domain. The offset is from 100 to 7900 meters with 200-meter increment.

Figure 5. Stacked migration from the initial velocity model. The rectangle marks show the distortion of subsurface image because of errors in the velocity model.

Figure 6. The selected common image gathers using the updated velocity model from the proposed integrated tomography after several iterations. The gathers are in the depth-offset domain. The offset is from 100 to 7900 meters with 200-meter increment.

Figure 7. The stacked migration using the updated velocity model from the proposed integrated tomography after several iterations. The rectangle marks show the distortion of subsurface image because of errors in the velocity model.

Figure 8. The updated velocity model from the proposed integrated tomography after several iterations. The circle shows the inverted overthrust feature corresponding to the true model.

Figure 9. The true velocity model derived from Canadian Foothill. This model is used to generate synthetic seismic shots for this study. The circle shows the overthrust.

Figure 10. The stacked migration using the true velocity model. The rectangle marks corresponding to ones in the other stacked sections.

Figure 11: A Schematic geological section for the studying area.

Figure 12. Elevation map of studying area. The white dash line presents inline ILA.

Figure 13a. Near-surface model derived from Turning-ray tomography at inline ILA.

Figure 13b. Depth slice at 900 m of near-surface model derived from turning-ray tomography,

Figure 14. Initial model combining both near-surface model derived from turning-ray tomography and legacy model.

Figure 15. Velocity before (left) and after (right) integrated tomography update.

Figure 16. Stacked PSDM overlaid with the initial (left) and inverted (right) anisotropic epsilons respectively.

Figure 17. Location of Well KS12 on a representative TTI PSDM section. The new apex of the structure (blue line cutting through) is several hundred meters away from the previously drilled location (yellow dashed line), suggesting a new well location. The left panel is the updated velocity overlaid by image and the right panel is image only.

Figure 18. Common image gathers located at several crosslines at inline ILA generated by PSDM using the initial models. The gathers are in the offset and depth domain. Some events curve down and others curve up.

Figure 19. Common image gathers located at several crosslines at inline ILA generated by PSDM using the updated anisotropic models. The gathers are in the offset and depth domain. The flatness of events improves significantly overall.

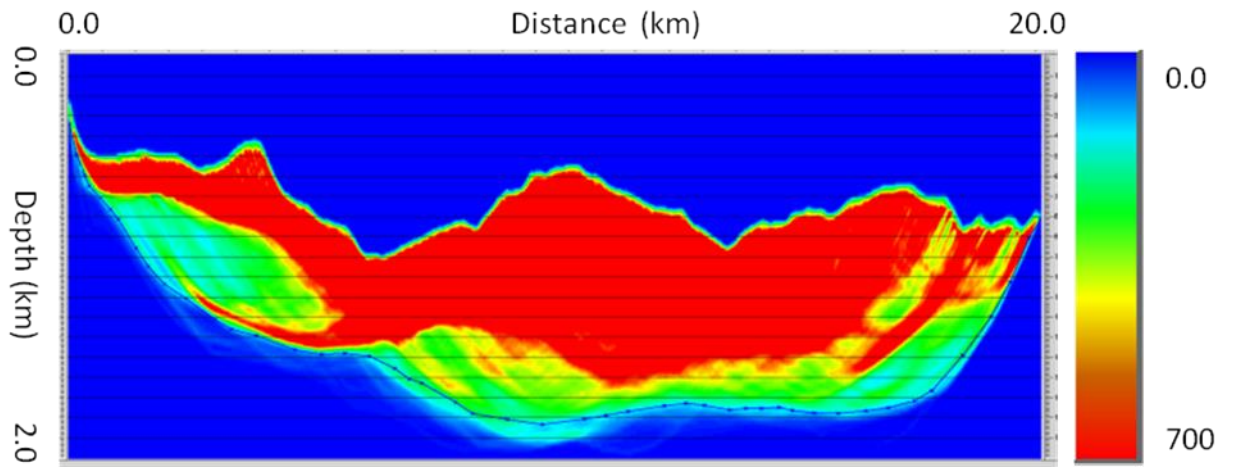


Figure 1. Ray density from turning-ray tomography. The dotted line in the deeper part is the horizon for maximum depth of reliable velocities.

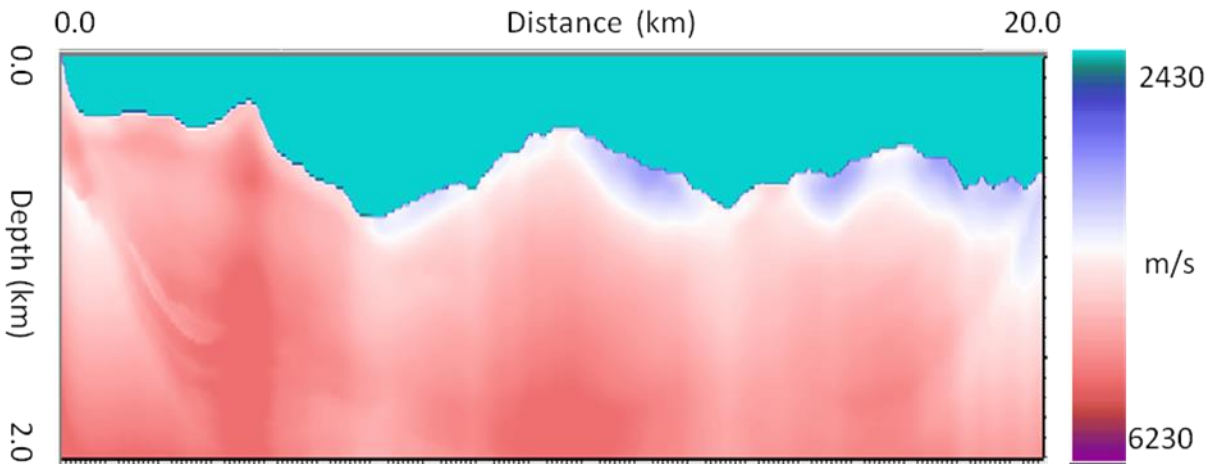


Figure 2. Inverted near surface model from turning-ray tomography.

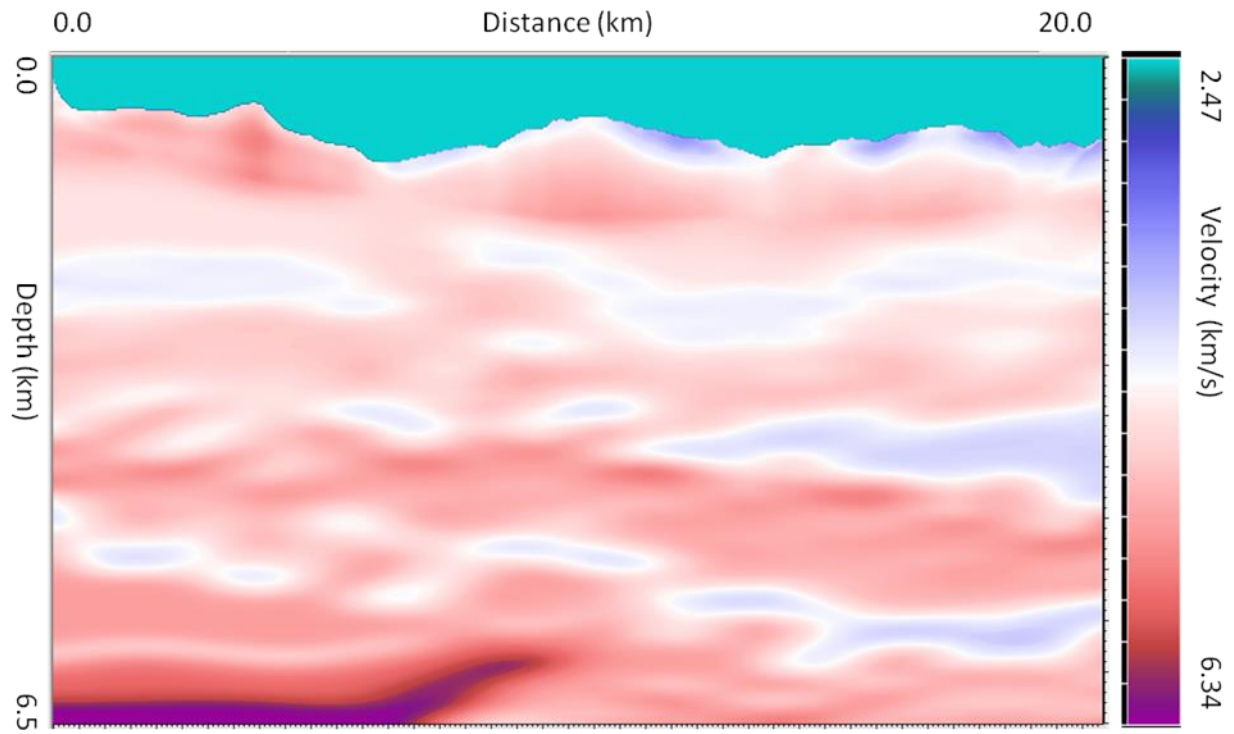


Figure 3. The combined initial model for reflection tomography. Shallow part is from the inverted near-surface model from turning-ray tomography; deep part is from the true velocity model with heavily smoothing and scaling.

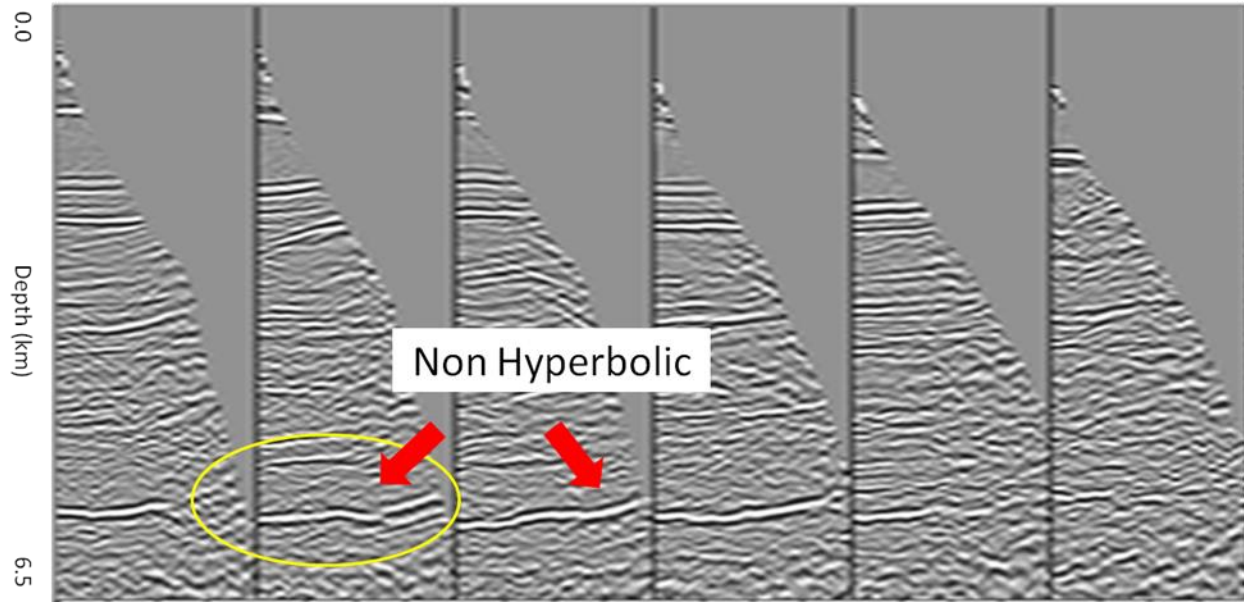


Figure 4. The selected common image gathers using the integrated initial velocity model. The arrows show the non-hyperbolic residual moveout. The gathers are in depth-offset domain. The offset is from 100 to 7900 meters with 200-meter increment.

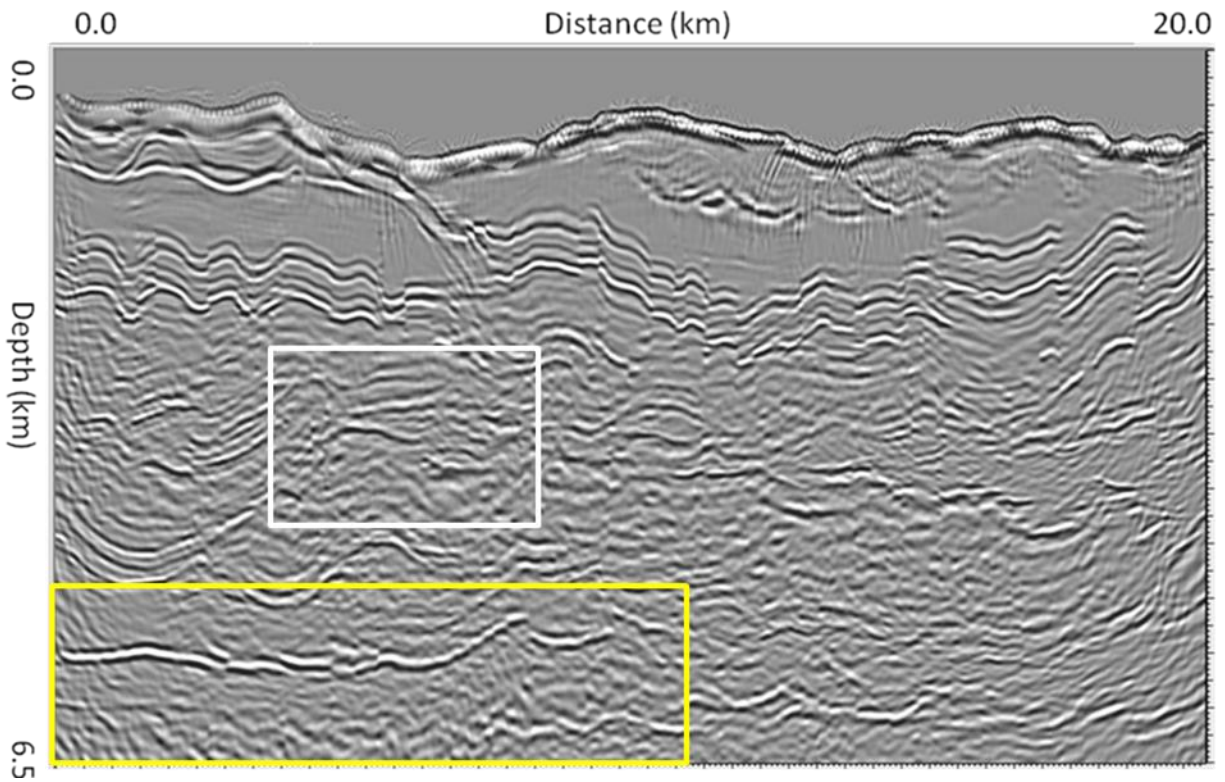


Figure 5. Stacked migration from the initial velocity model. The rectangle marks show the distortion of subsurface image because of errors in the velocity model.

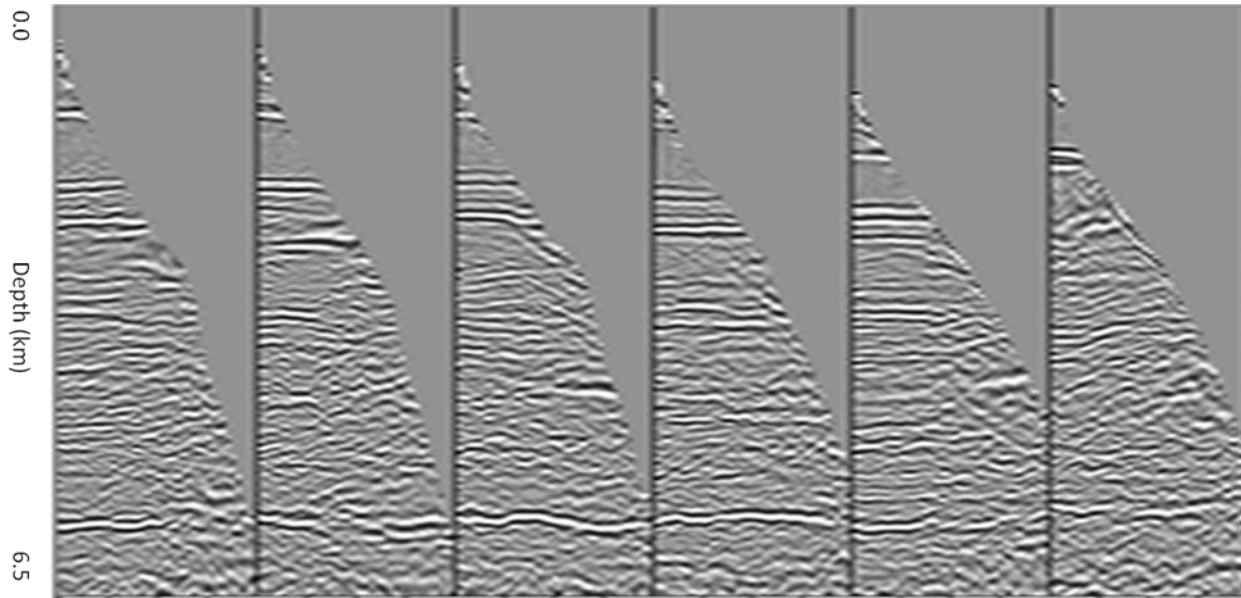


Figure 6. The selected common image gathers using the updated velocity model from the proposed integrated tomography after several iterations. The gathers are in depth-offset domain. The offset is from 100 to 7900 meters with 200-meter increment.

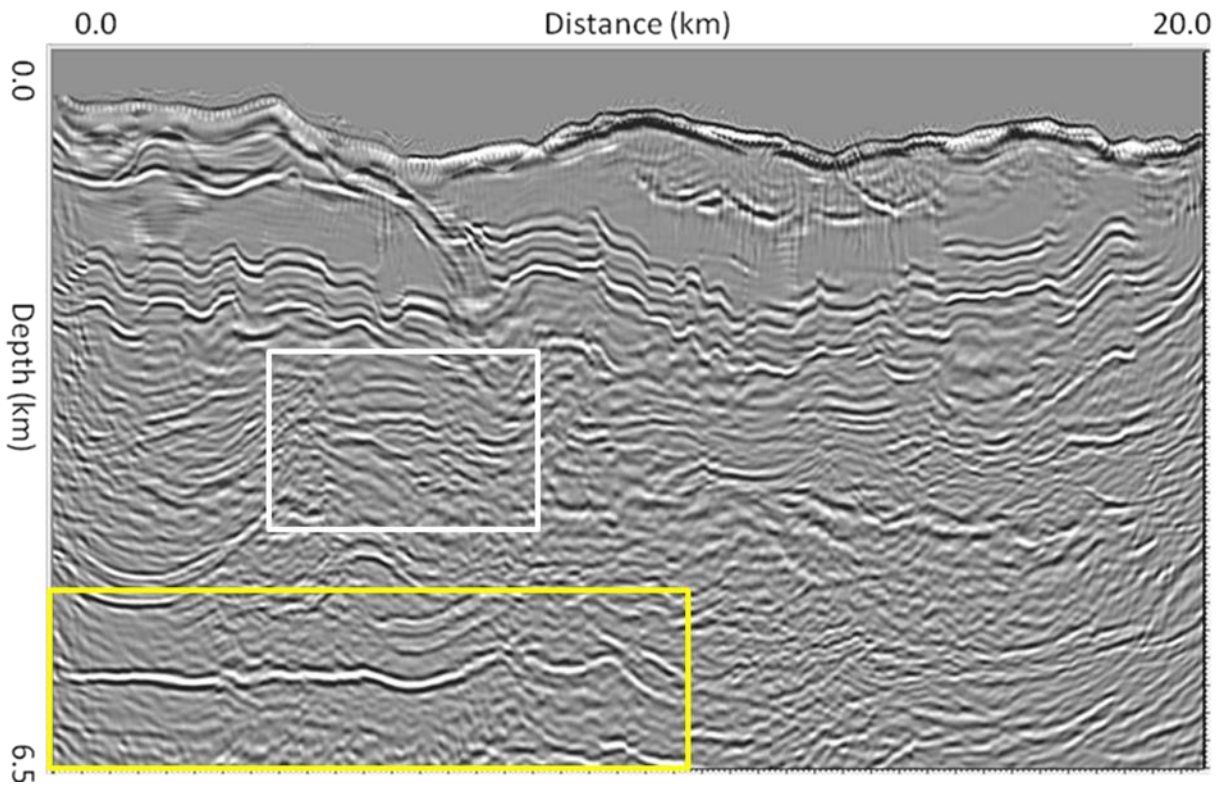


Figure 7. The stacked migration using the updated velocity model from the proposed integrated tomography after several iterations. The rectangle marks show the distortion of subsurface image because of errors in the velocity model.

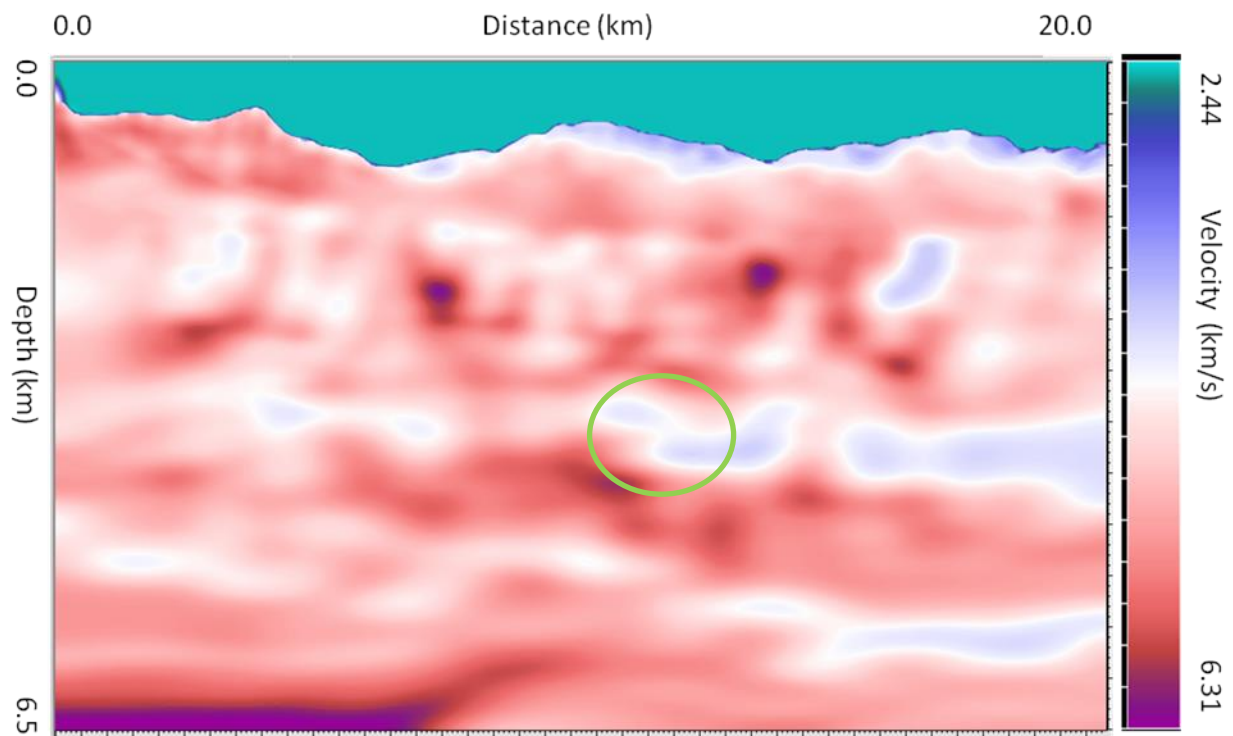


Figure 8. The updated velocity model from the proposed integrated tomography after several iterations. The circle shows the inverted overthrust feature corresponding to the true model.

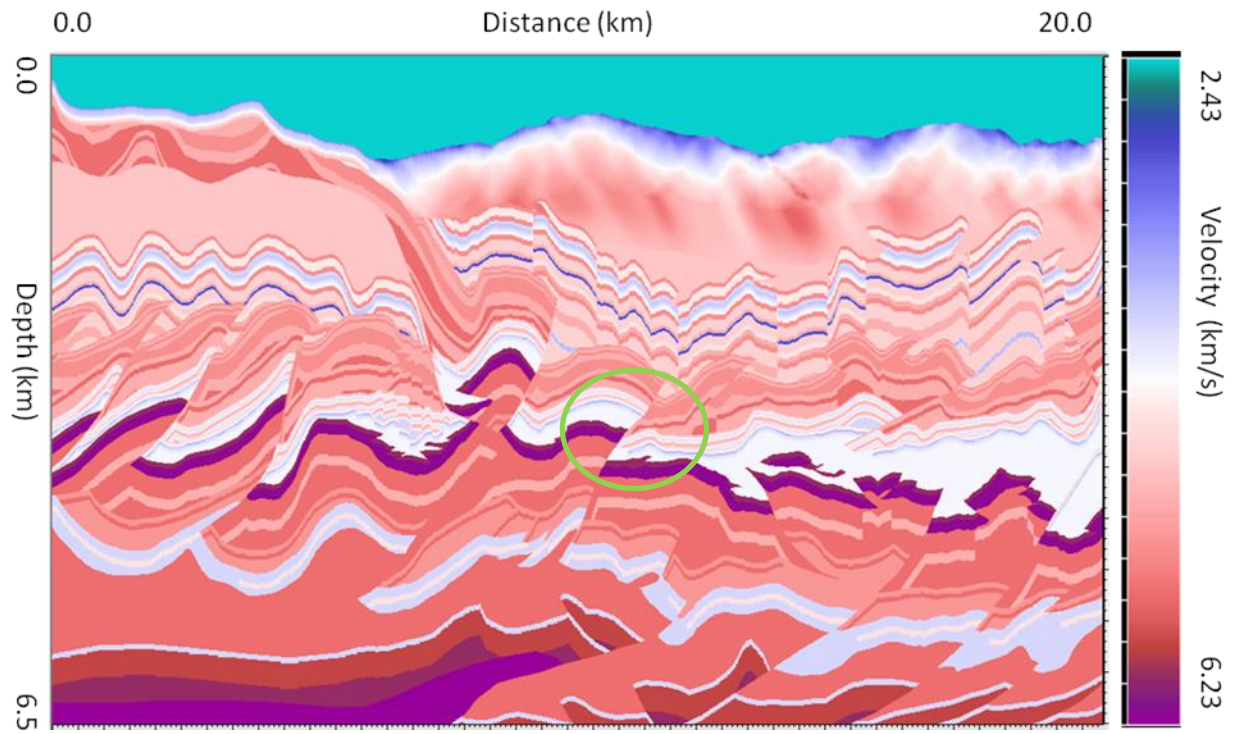


Figure 9. The true velocity model derived from Canadian Foothill. This model is used to generate synthetic seismic shots for this study. The circle shows the overthrust.

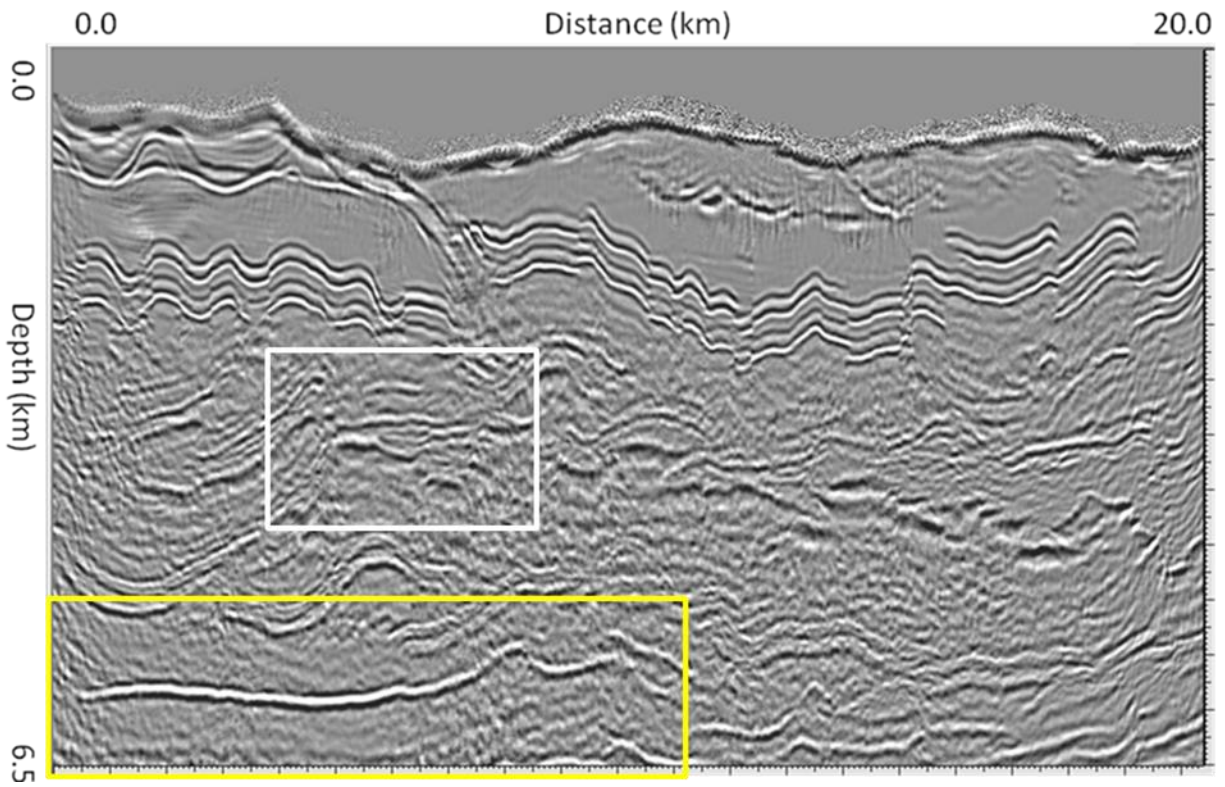


Figure 10. The stacked migration using the true velocity model. The rectangle marks corresponding to ones in the other stacked sections.

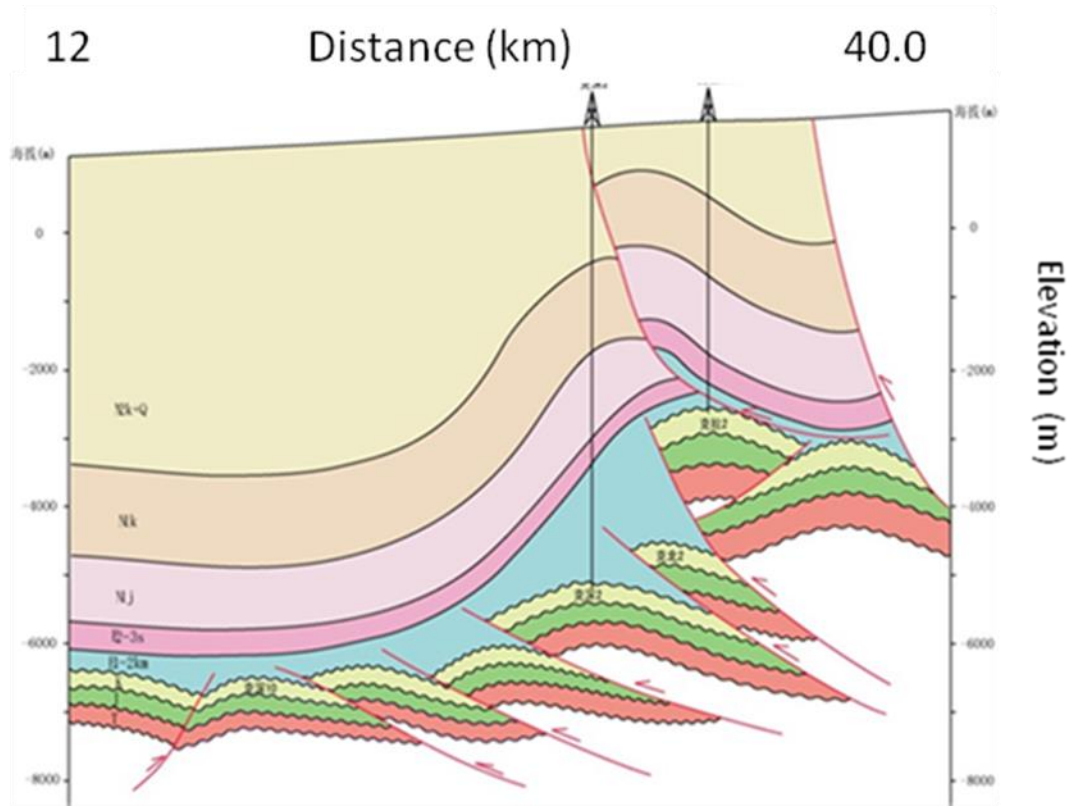


Figure 11: A Schematic geological section for the studying area.

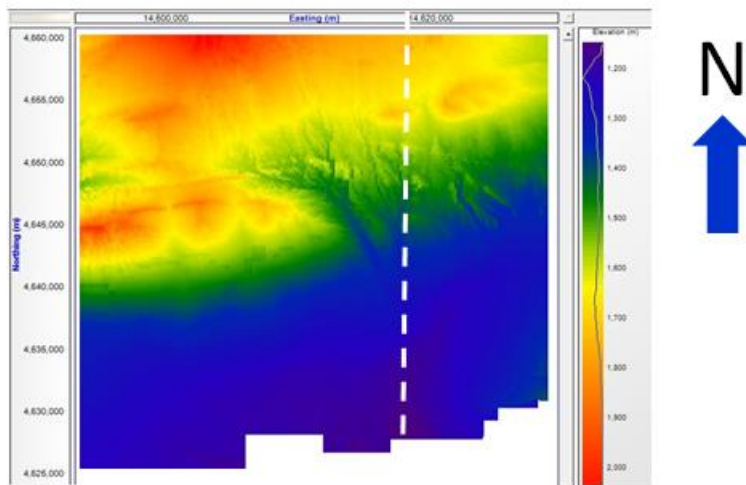


Figure 12. Elevation map of studying area. The white dash line presents inline ILA.

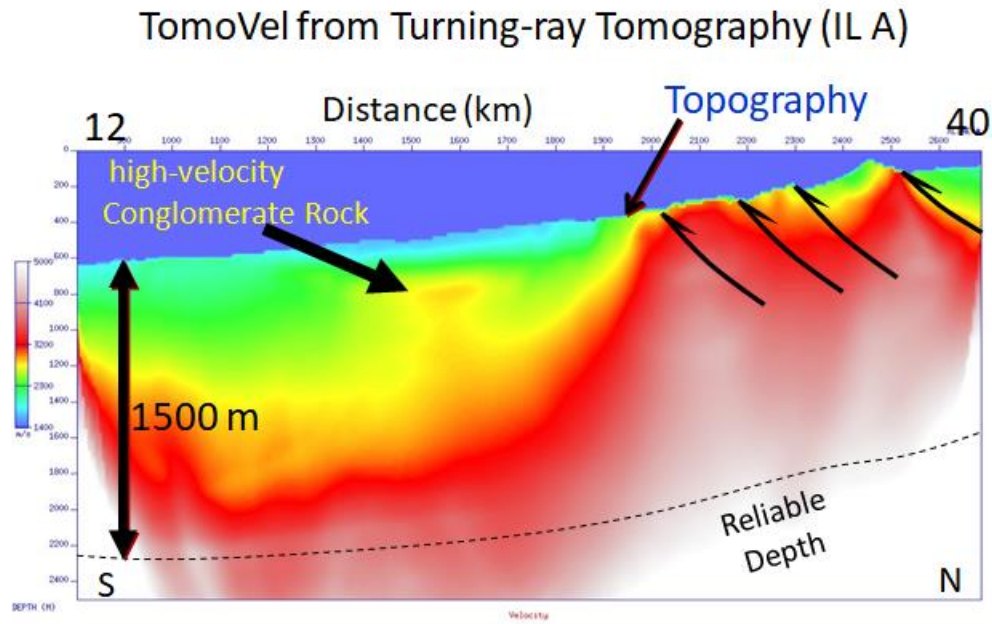


Figure 13a. Near-surface model derived from Turning-ray tomography at inline ILA.

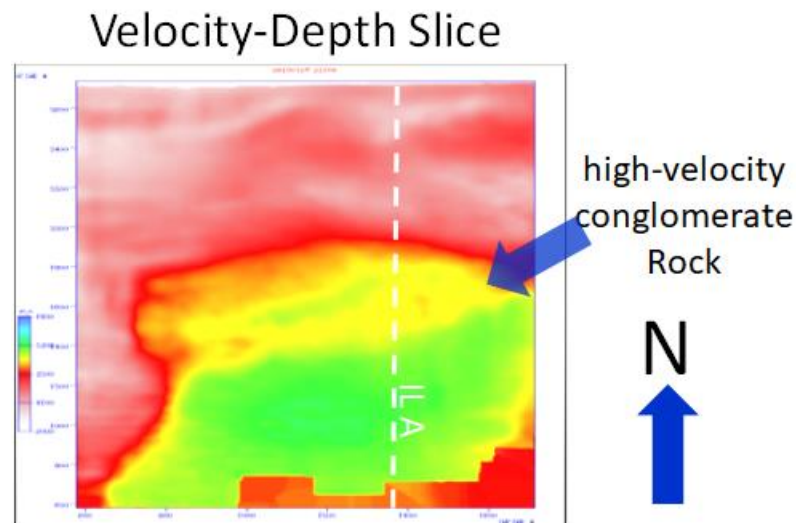


Figure 13b. Depth slice at 900 m of near-surface model derived from turning-ray tomography,

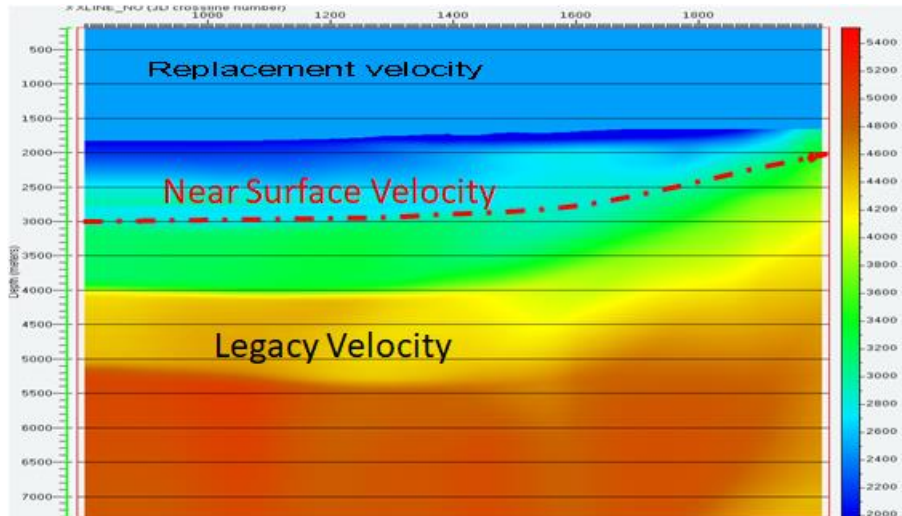


Figure 14. Initial model integrating both near-surface model derived from turning-ray tomography and legacy model.

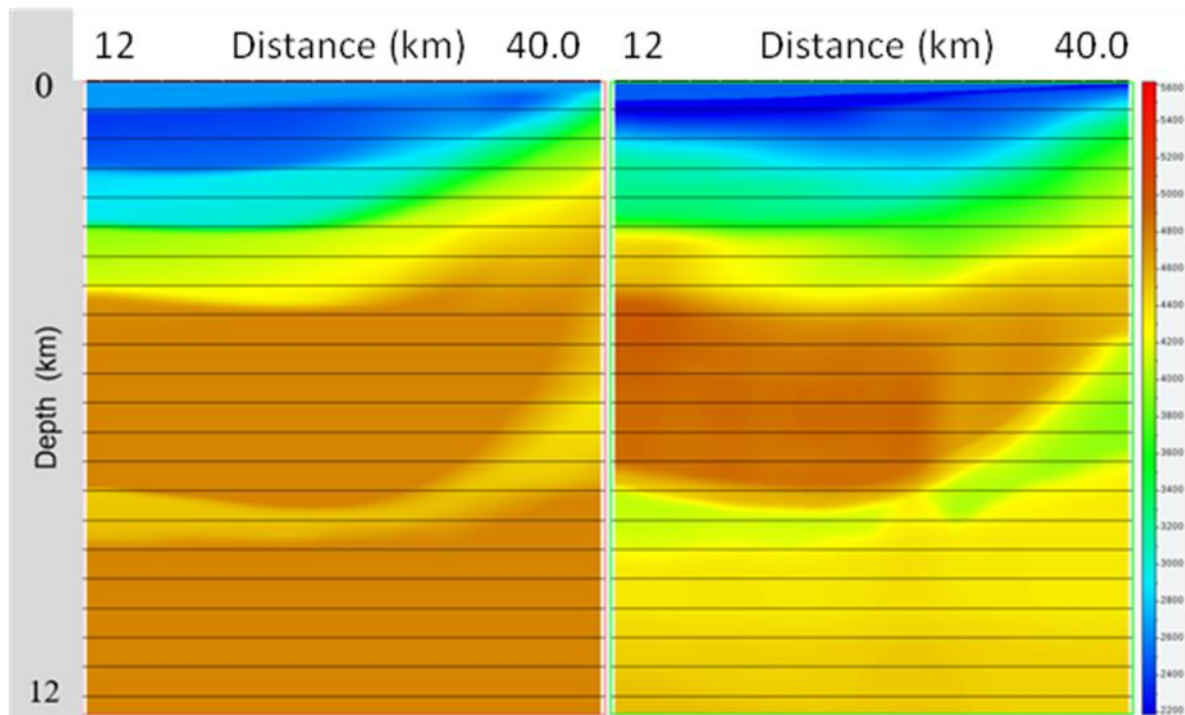


Figure 15. Velocity before (left) and after (right) TTI tomography update integrated with the near-surface model derived from turning-ray tomography.

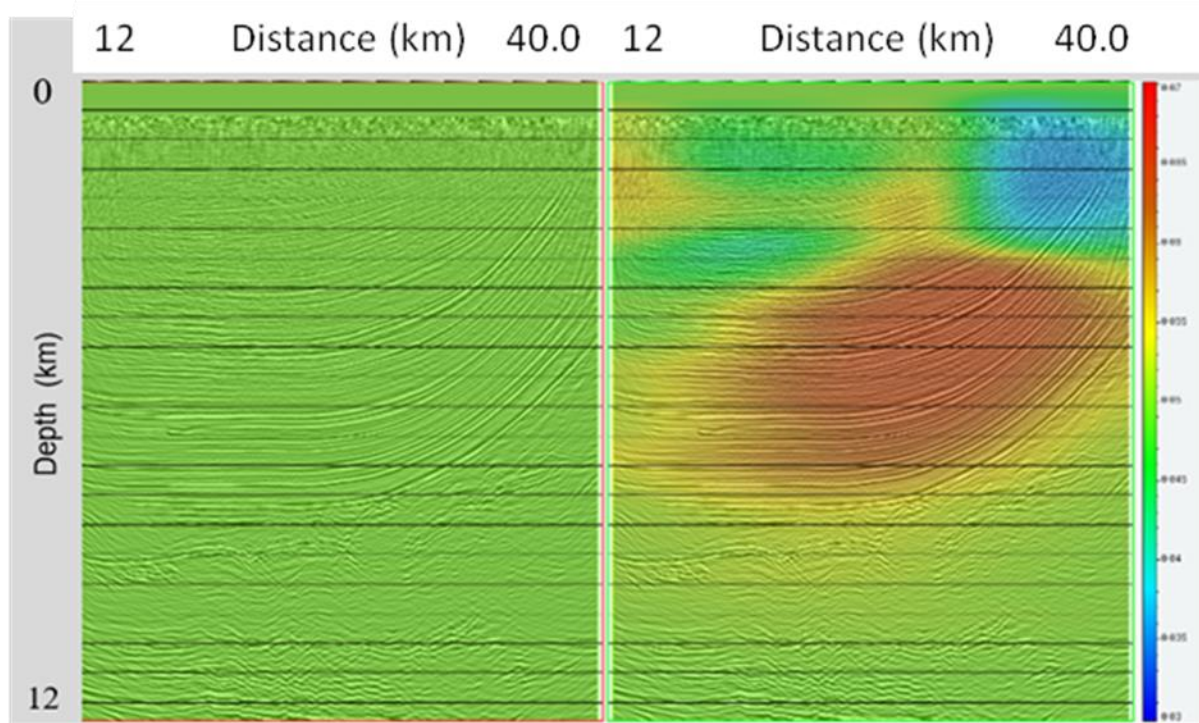
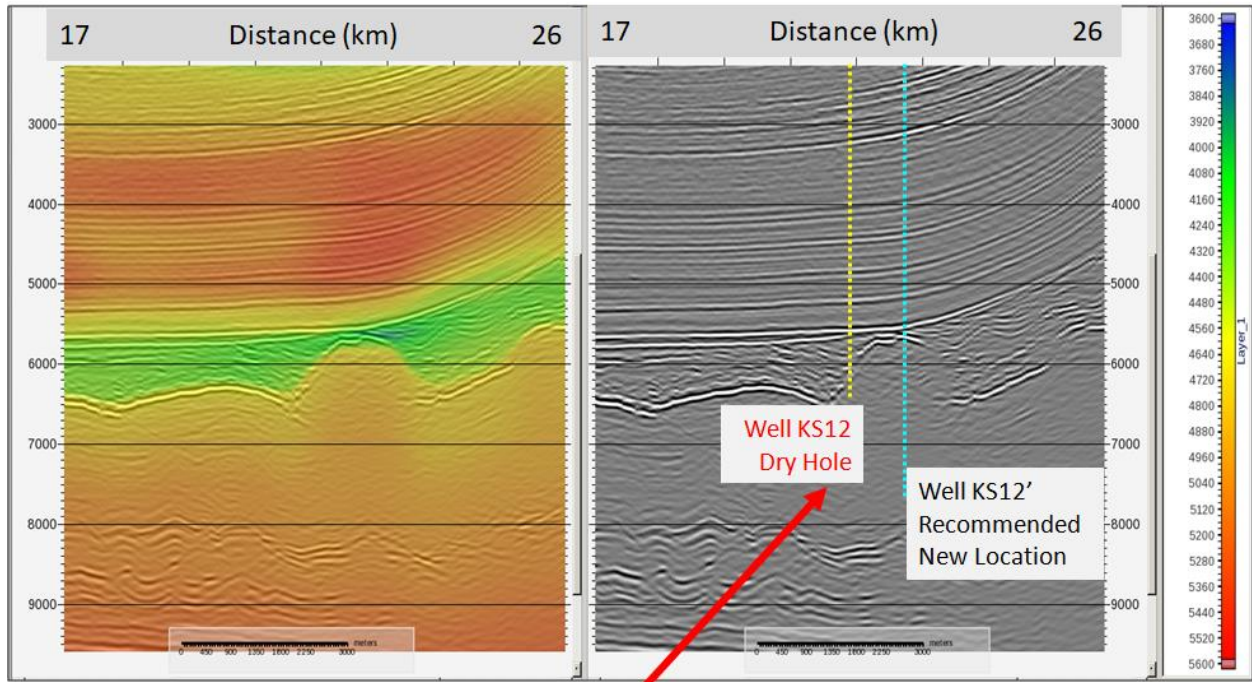


Figure 16. Stacked PSDM overlaid with the initial (left) and inverted (right) anisotropic epsilons respectively.



After reprocessing: KS12 well was not drilled on the structural high

Figure 17. Location of Well KS12 on a representative TTI PSDM section. The new apex of the structure (blue line cutting through) is several hundred meters away from the previously drilled location (yellow dashed line), suggesting a new well location. The left panel is the updated velocity overlaid by image and the right panel is image only.

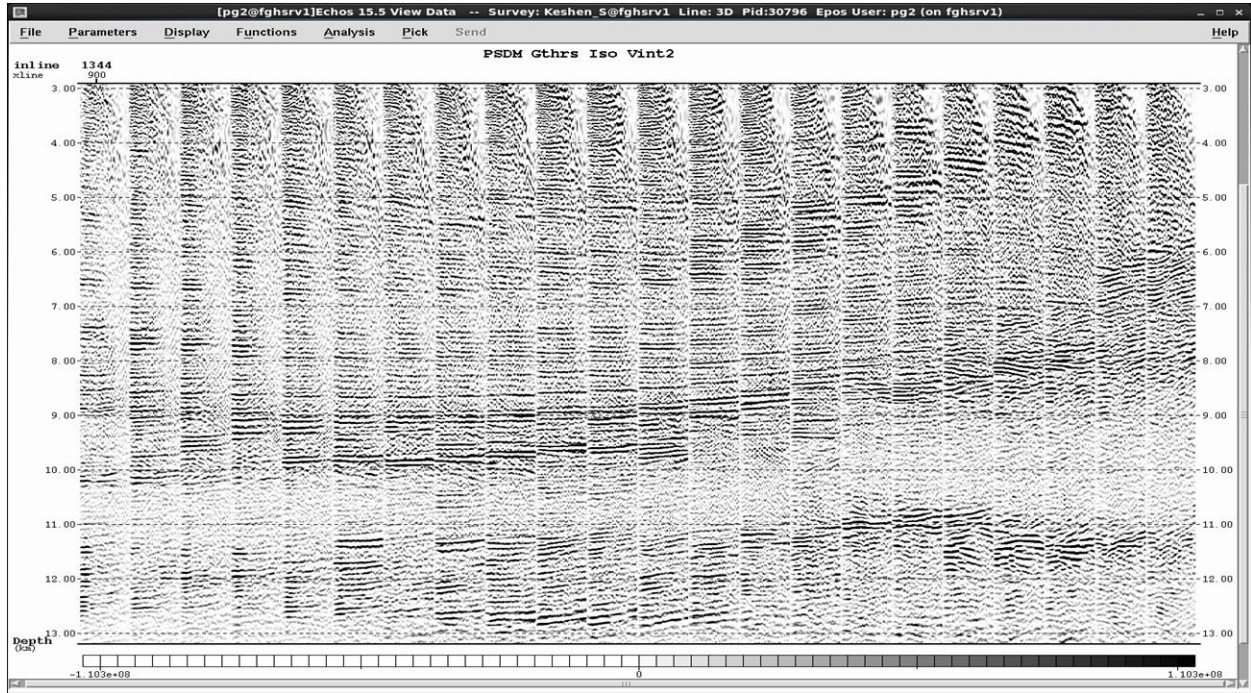


Figure 18. Common image gathers located at several crosslines at inline ILA generated by PSDM using the initial models. The gathers are in the offset and depth domain. Some events curve down and others curve up.

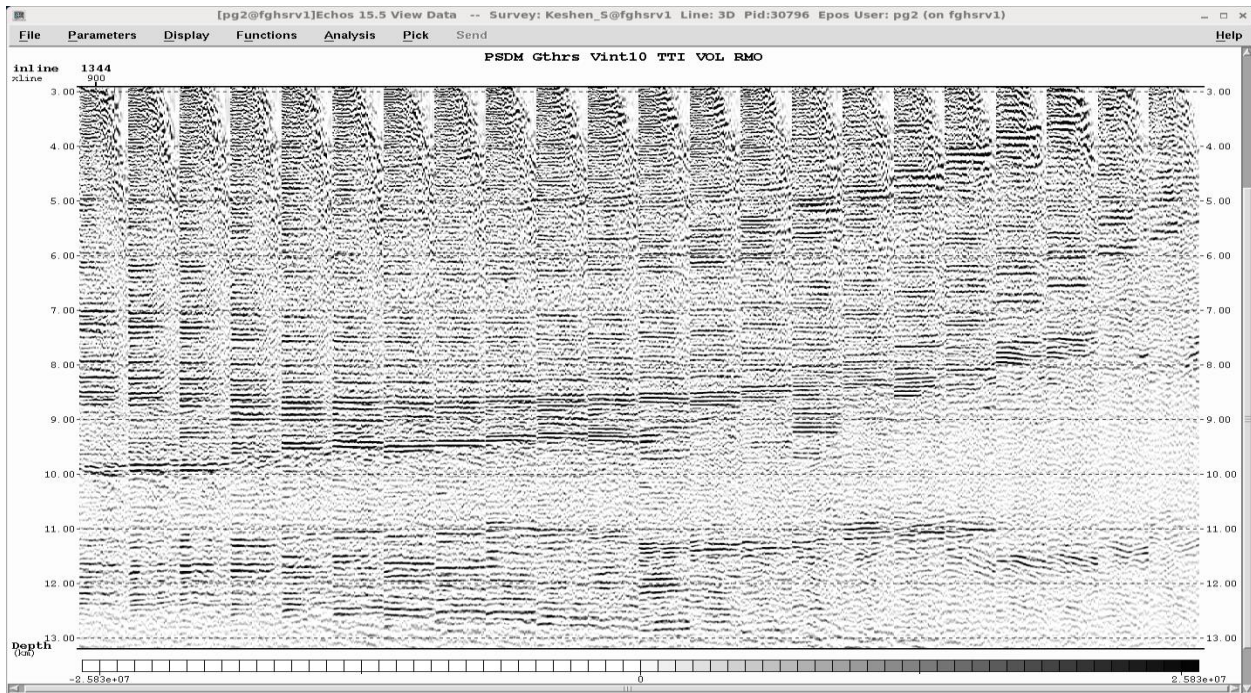


Figure 19. Common image gathers located at several crosslines at inline ILA generated by PSDM using the updated anisotropic models. The gathers are in the offset and depth domain.

The flatness of events improves significantly overall.